High-resolution distributed shape sensing using phase-sensitive optical time-domain reflectometry and multicore fibers

Łukasz Szostkiewicz,[1,2,4,*] Marcelo A. Soto,[1,5] Zhisheng Yang,[1] Alejandro Dominguez-Lopez,[2] Itxaso Parola,[2] Krzysztof Markiewicz,[2] Anna Pytel,[2,3] Agnieszka Kołakowska,[2,3] Marek Napierała,[2] Tomasz Nasiłowski,[2] and Luc Thevenaz[1]

[1]*EPFL Swiss Federal Institute of Technology, Institute of Electrical Engineering, SCI STI LT, Station 11, CH-1015 Lausanne, Switzerland*
[2]*InPhoTech sp. z o.o., ul. Dzika 12/15, 00-172 Warsaw, Poland*
[3]*Polish Centre for Photonics and Fibre Optics, Al. Racławickie 8 lok 12, 20-037 Lublin, Poland*
[4]*Faculty of Physics, Warsaw University of Technology, ul. Koszykowa 75, 00-662 Warsaw, Poland*
[5]*Permanent address: Department of Electronic Engineering, Universidad Técnica Federico Santa María, 2390123 Valparaíso, Chile*
[*]*lszostkiewicz@inphotech.pl*

Abstract: In this paper, a highly-sensitive distributed shape sensor based on a multicore fiber (MCF) and phase-sensitive optical time-domain reflectometry (φ-OTDR) is proposed and experimentally demonstrated. The implemented system features a high strain sensitivity (down to $\sim$0.3 $\mu\varepsilon$) over a 24 m-long MCF with a spatial resolution of 10 cm. The results demonstrate good repeatability of the relative fiber curvature and bend orientation measurements. Changes in the fiber shape are successfully retrieved, showing detectable displacements of the free moving fiber end as small as 50 μm over a 60 cm-long fiber. In addition, the proposed technique overcomes cross-sensitivity issues between strain and temperature. To the best of our knowledge, the results presented in this work provide the first demonstration of distributed shape sensing based on φ-OTDR using MCFs. This high-sensitivity technique proves to be a promising approach for a wide range of new applications such as dynamic, long distance and three-dimensional distributed shape sensing.

1. Introduction

Distributed optical fiber sensors (DOFSs) offer the possibility to monitor a variety of parameters (e.g. strain, temperature, vibration, etc.) continuously along the entire length of an optical fiber with a very sharp spatial resolution [1]. Due to these unprecedented features, DOFSs are seen to be the most suitable and promising technology for monitoring large structures using an optical fiber as they provide a vast number of independent sensing points. The working principle of these sensors is based on the analysis of the scattered light within the optical fiber due to either Rayleigh, Brillouin or Raman scattering [2]. Whilst in recent years DOFSs have evolved dramatically, resulting in an increase in the sensing resolution and a reduction in measurement times [3–5], the vast majority of them have been confined to measuring strain and/or temperature profiles. The main reason for concentrating so much on these two parameters is the relatively low insensitivity of conventional single-mode optical fibers (ITU-T G.652) to other physical quantities. However, due to the recent development of specialty optical fibers like few-mode fibers [6], photonic crystal fibers [7,8] and hollow-core fibers [9], the breadth of potential applications for DOFSs has got enlarged. The synergy between specialty optical fibers and DOFSs makes it now possible

to measure parameters that cannot be measured with the use of standard single-mode fibers, such as pressure sensing [10], axial stress sensing [11], or gas concentration [12]. On the other hand, multicore fibers (MCFs) were initially developed to face the capacity crunch of the optical fiber networks based on single-core fibers [13]. The combination of MCFs with mode-division multiplexing techniques has demonstrated an extraordinary potential to increase the transmission capacity of optical fiber links [14]. However, due to the unique features of MCFs, they have also found a niche market in the field of optical fiber sensing. They have been used successfully as bending and curvature sensors [15,16], and in applications such as accelerometers [17] and velocity sensors [18]. Nevertheless, one of the most promising sensing applications for MCFs is the monitoring of the shape of an optical fiber (shape sensing) by analyzing the differential strain distribution along its different cores. The first demonstration of a time domain analysis distributed shape sensor on MCFs was recently published by Zhao et al., where the Brillouin optical time domain analysis (BOTDA) technique was employed to extract the fiber shape [19]. However, other distributed sensing techniques that present a higher sensitivity than BOTDA have not yet been explored for this application. One of these techniques is the so-called phase-sensitive optical time domain reflectometry (φ-OTDR), which has a sensitivity level that is three orders of magnitude superior to that of BOTDA [20]. It is therefore expected that much more sensitivity to shape variations can be achieved by performing φ-OTDR measurements over MCFs.

In this paper, a novel highly-sensitive distributed shape sensor is proposed based on φ-OTDR measurements over a MCF. Making use of the differential strain distribution of three cores of a MCF, displacement measurements with extremely high precision and high spatial resolution have now been experimentally demonstrated for the first time, to the best of our knowledge. Measurements of relative strain and calculations of the absolute curvature and bend orientation of the fiber are carried out, confirming good repeatability in all cases. Changes in the fiber shape are calculated and illustrated, showing the capability to detect changes at a sub-millimeter scale, being as small as 50 µm over a 60 cm-long fiber span. The results presented in this work positively contribute to the promising development of distributed curvature and bending sensors based on φ-OTDR in MCFs, and pave the way to the implementation of a wide range of new applications, such as dynamic, long range and three-dimensional distributed shape-sensing.

As of today, long range optical fiber sensors do not allow to perform efficient modal analysis of long structures like bridges or buildings. Such situation is caused by the fact that one cannot measure the direction of the deformation with high enough repetition rate in distributed manner. Technique proposed and described below may be applicable for creating multi km distributed vibration meter that gives the information not only about the amplitude of vibration but also about its direction. Full information about movement of the infrastructure is a key for securing safety of operation.

2. Shape sensing with multicore optical fibers

By measuring simultaneously the strain deviations of several cores within a MCF, whose geometry is known, it is possible to extract the information about the curvature over each differential section of the fiber [19]. In this study, a hole-assisted 7-core multicore fiber fabricated by InPhoTech is used, with a central core and 6 outer cores arranged in a hexagonal array [see Fig. 1(a)]. This fiber has an outer diameter of 135 µm, a core pitch d of 40 µm, and each core properties are in line with ITU-T G.652 recommendation. Any three cores that are not arranged in a straight line are sufficient to perform the analysis presented here. The three cores selected in this work and the pitch distance d are depicted in Fig. 1(a). On the other hand, Fig. 1(b) represents an analytical drawing of the cross section of the MCF in two different scenarios. The bottom representation corresponds to the original position of the fiber, which is used as a reference for the rest of the measurements. In this position, the three cores under test (C1, C2 and C3) lie on the XY plane. The upper drawing represents the MCF subjected to a differential strain over the

fiber cross-section, as caused by a bending. In this case, the cores lie within a plane tilted by a certain angle with respect to the reference, and their position is denoted as P1, P2 and P3. Their coordinates are defined as:

$$P_i = (d \cos \theta_i, d \sin \theta_i, \varepsilon_i), \tag{1}$$

where θ_i represents angles between the i-th core and the x axis, and ε_i represents the strain induced in the i-th core. The coordinates of the central core position are defined as $P0 = (0, 0, \varepsilon_{const.})$, where $\varepsilon_{const.}$ is the common strain that all the cores undergo. At this point it is worth mentioning that $\varepsilon_{const.}$ effect is the same like temperature effect. Since factor $\varepsilon_{const.}$ is not influencing both curvature and bending orientation calculation, one can claim that the measurement is inherently insensitive to temperature. This stays true if two conditions are fulfilled: all the cores at given position exhibit the same temperature and all the cores are measured at the same time. In the same way, one can define the location of a certain point $P = (d \cos \theta_b, d \sin \theta_b, \varepsilon_b + \varepsilon_{const.})$, where θ_b represents the bending orientation and $\varepsilon_b = dk$ is the strain induced by such bending at the location of the point P (where $k = 1/R$ is the curvature associated with a given bending radius R). Point P can be associated to a fictive core positioned exactly in the bending direction.
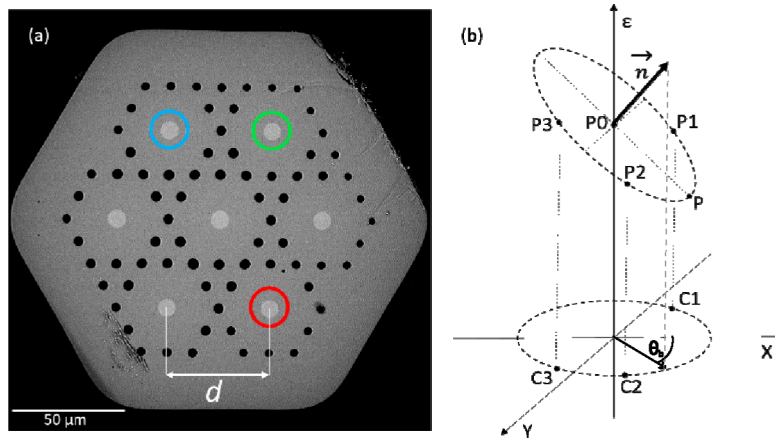

Fig. 1. (a) Cross-section of the 7-core MCF used in the experiment. The colored circles indicate the three cores selected for this analysis: red (bottom right): Core 2; blue (top left): Core 4; green (top right) Core 5. (b) Analytical drawing of the MCF in two different scenarios: bottom: origin position with all the cores within the XY plane; top: position subjected to a bend with the cores displaced within a plane tilted by a certain angle with respect to the reference position. Points C1, C2, C3 represent the fiber cores coordinates in fiber cross section (XY plane). Points P0, P1, P2, P3 represent the fiber cores coordinates (XY plane) and the measured strain value in each core. Vector $\vec{n}$ is a normal vector to a plane fitted to the measured coordinates of P1, P2, P3. Point P represents the coordinates of a fictive core positioned in the bending direction. θ_b is the bending orientation of the fiber which is in line with the projection of the $\vec{n}$ vector on the XY axis.

To calculate the position of point P, a normal vector $\vec{n} = (n_x, n_y, n_z)$ is defined from the plane formed by $P1$, $P2$ and $P3$, satisfying that $\vec{n} = (P2 - P1) \times (P3 - P1)$. Then, based on the x and y coordinates of the normal vector $\vec{n}$, the bending orientation θ_b is defined as:

$$\theta_b = arctan \frac{n_y}{n_x}. \tag{2}$$

The projection of vector $\vec{n}$ to XY plane (which is defined by fiber geometry) points at the same direction as bending orientation θ_b. As the x and y coordinates of point P are known (due to

the known structure of the fiber), as well as the plane in which it is lying (given by the normal vector $\vec{n}$), the exact position of the point P can be determined by knowing the bending orientation. Hence, the equation of the plane for this point can be defined as:

$$0 = n_x d \cos \theta_b + n_y d \sin \theta_b + n_z \varepsilon_b. \tag{3}$$

Then, solving for the only unknown ε_b, the strain induced by bending can be written as:

$$\varepsilon_b = -\frac{n_x}{n_z} d \cos \theta_b - \frac{n_y}{n_z} d \sin \theta_b, \tag{4}$$

and the curvature of the fiber can be calculated directly from the strain as:

$$k = |\varepsilon_b / d|. \tag{5}$$

Finally, the shape change of the fiber can be retrieved by means of the well-known Frenet-Serret formulas [21,22]. As mentioned above, the methodology presented in this section is applicable to any initial choice of three cores, as long as they are not arranged in a straight line within the geometry of the MCF.

3. Experimental setup

The experimental setup employed in this work is shown in Fig. 2, which corresponds to a classical high-performance implementation of a φ-OTDR sensor [20]. In this case, a distributed-feedback (DFB) laser is used as a light-source, and the wavelength sweeping is carried out by tuning the bias current of the DFB laser. In a first step, the output pulse is shaped by means of a Mach-Zehnder electro-optical intensity modulator (EOM), obtaining a probe pulse of ~ 1 ns, which corresponds to a spatial resolution of 10 cm. The pulse waveform is externally shaped by an electrical arbitrary waveform generator (AWG). To secure a sufficiently high extinction ratio (ER) of the probe pulses, a second EOM is employed to gate the pulses, and hence, to further reduce the out-of-pulse Rayleigh backscattered power (which provides no useful information and potentially distorts the measurements). Then, the probe pulse power is boosted by means of an erbium-doped fiber amplifier (EDFA). This amplification stage is followed by a variable optical attenuator (VOA), which is used to accurately adjust the power launched into the sensing fiber and to avoid non-linear effects such as modulation instability in the MCF [23]. After passing through a circulator and before entering the fiber, an optical switch (OS) is inserted to enable comparable measurements between the cores of interest in an automated manner. A fan-in/fan-out (Fi/o) device (maximum insertion losses of ~ 1.1 dB for each core) is connected to the output of the OS, and it serves to couple the light from seven single-mode fibers to each core of the MCF. The backscattered light within the fiber under test (FUT) comes out from port three of the circulator and is amplified by means of an EDFA, thus enabling sufficient power to reach the detector. The amplified spontaneous emission of the EDFA is filtered by a tunable band-pass optical filter (BPOF), which isolates the signal of interest and limits the sources of noise. A photodiode (PD) is used as a detector, which features a bandwidth of 3 GHz (enough to perform measurements with a spatial resolution of 10 cm). As a final step, the electrical signal generated by the PD is acquired by an oscilloscope with 4 GHz bandwidth.

The arrangement of the displacement setup is illustrated in Fig. 3. As can be seen, the MCF is fixed to the base at point A, which limits the length of the moving section of the fiber (segment AB) to ~ 60 cm and ensures that comparable measurements are made. The fiber was placed in protective tape in an non-twisted state at its whole length. The MCF is also attached to a computer-controlled translation stage (point B in Fig. 3) elevated 31.3 cm from the base. Two precisely measured physical dimensions (35,5 cm and 12,8 cm) indicate the level of initial tension applied to the fiber. Due to the high sensitivity of the system, the moving stage is set to shift
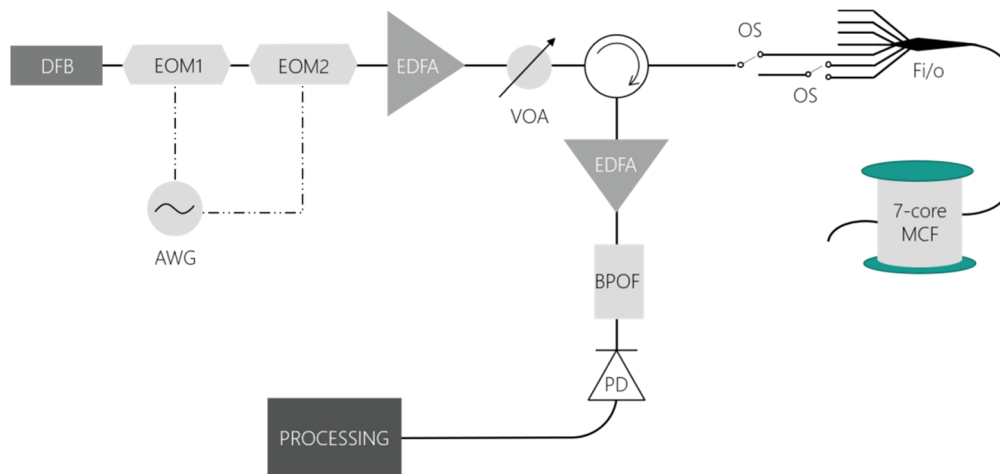
Fig. 2. Experimental setup of the phase-sensitive OTDR. DFB: distributed-feedback laser; EOM: electro-optical modulator; AWG: arbitrary waveform generator; EDFA: erbium-doped fiber amplifier; VOA: variable optical attenuator; OS: optical switch; Fi/o: fan-in/fan-out; MCF: multi-core fiber; BPOF: band-pass optical filter; PD: photodiode.

upwards and downwards by steps of 2 mm, with a total vertical displacement range of 2 cm. The total fiber length of the MCF is ~ 24 m. Since range limiting factors for φ-OTDR setup are: pulse power, extinction ratio of the pulse and loss of the fiber the measurement range can be easily extended beyond 24 m of length to km range.
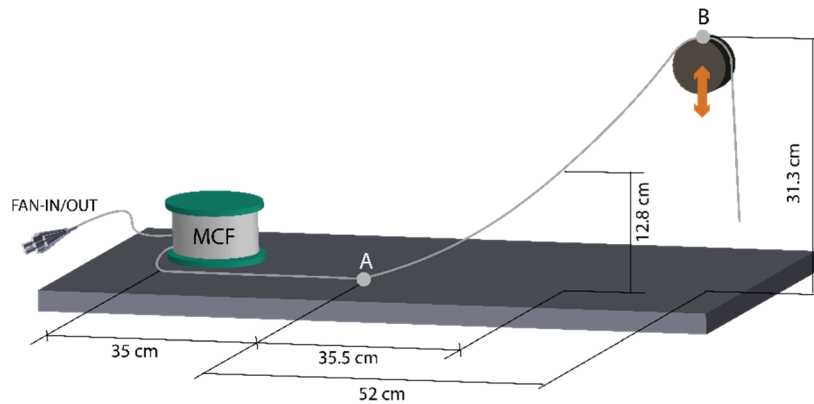

Fig. 3. Displacement setup. The MCF is attached to the base at point A, and from there ~ 60 cm of fiber are suspended in the air up to point B, fixed to a vertical translation stage.

To ensure that the measured traces allows for a sufficient contrast to properly extract the strain measurements, a high visibility is necessary. The visibility is defined as:

$$Visibility = \frac{I_{max} - I_{min}}{I_{max} + I_{min}}, \tag{1}$$

where I_{max} and I_{min} are respectively the maximum and the minimum intensity of the trace [24]. An example of the measured trace and the calculated visibility is shown in Fig. 4(a), where the visibility is above 0.7 along the trace. The first section with a higher signal intensity (from 0 to 7 m) corresponds to the optical components used to address each particular core of the MCF.

An example of the calculated cross-correlation spectrum between two different measurements corresponding to two different heights (0 and 10 mm) of the moving stage for one core is illustrated in Fig. 4(b). As can be seen, there is a clearly visible shift (1.15 GHz) of the maximum peak as a result of the induced strain.
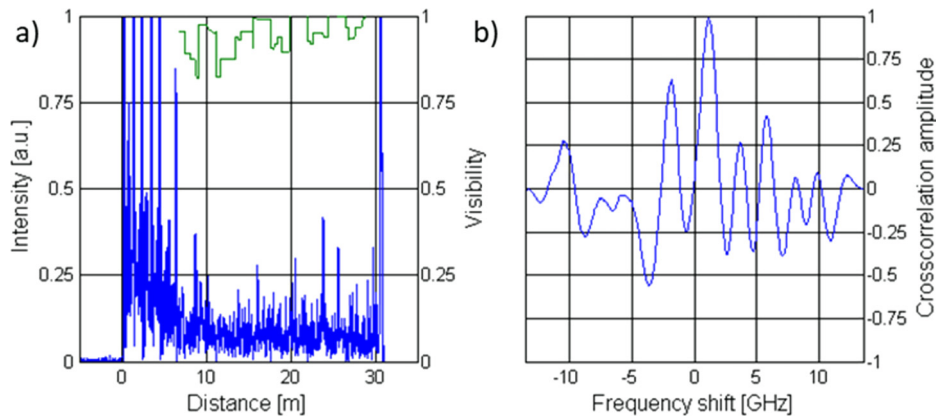

Fig. 4. (a) Example of the measured time trace for one of the cores of the MCF (blue line) and the calculated visibility for it (green line). (b) Example of the calculated cross-correlation spectrum between two different measurements corresponding to two different heights of the moving stage for one core.

4. Shape sensing results

In order to measure the accumulated strain (ε_b) along the fiber, a series of frequency sweeps were performed at each vertical position of the fiber (point B in Fig. 3). The frequency of the DFB laser is swept in steps of 50 MHz, until covering a total frequency scanning range of 13.5 GHz. Based on the strain sensitivity of silica fibers [20], this scanning frequency range provides a full dynamic range of 89 $\mu\varepsilon$. Note that the strain is estimated as the sum of the computed strains resulting from each increment in vertical position (relative strain values). Figure 5 illustrates the accumulated strain obtained in three of the cores with upward and downward displacements shown in 3D [Figs. 5(a) and 5(c)] and in a 2D cut for a vertical displacement of 18 mm [Figs. 5(b) and 5(d)]. As expected, there exists a strong correlation between the results obtained for both directions of displacements. Upward and downward movement experience different sign of strain measurement. Such sign change is not visible in Fig. 5(a) and 5(b) because vertical displacement is referenced only with positive values in respect to the initial position. It can be noted that the accumulated strain for the three cores is null up to the distance of 23 m, where the fiber is fixed to the base (point A in Fig. 3). Hence, as expected, no strain variations are measured before this position. From 23 m to ~ 23.16 m, the Core 2 (red) experiences a positive strain (elongation), whereas Cores 4 and 5 (blue and green respectively) undergo a negative strain (compression). At ~ 23.16 m there is a change in the curvature of the fiber (inflection point), and therefore, no strain or compression is induced in any of the cores at that point. Subsequently, from ~ 23.16 m to 23.6 m (point B in Fig. 3), Core 2 experiences a negative strain or compression, whilst Cores 4 and 5 are subject to a positive strain or elongation. Interestingly, a symmetrical behavior of Cores 2 and 4 (red and blue respectively) can clearly be observed in both Figs. 5(b) and 5(d), from which their opposing locations within the geometry of the MCF can be inferred [see Fig. 1 (a)]. It should be emphasized that the strong correlation between these two graphs reinforces the confidence in the presented technique and the implemented system.
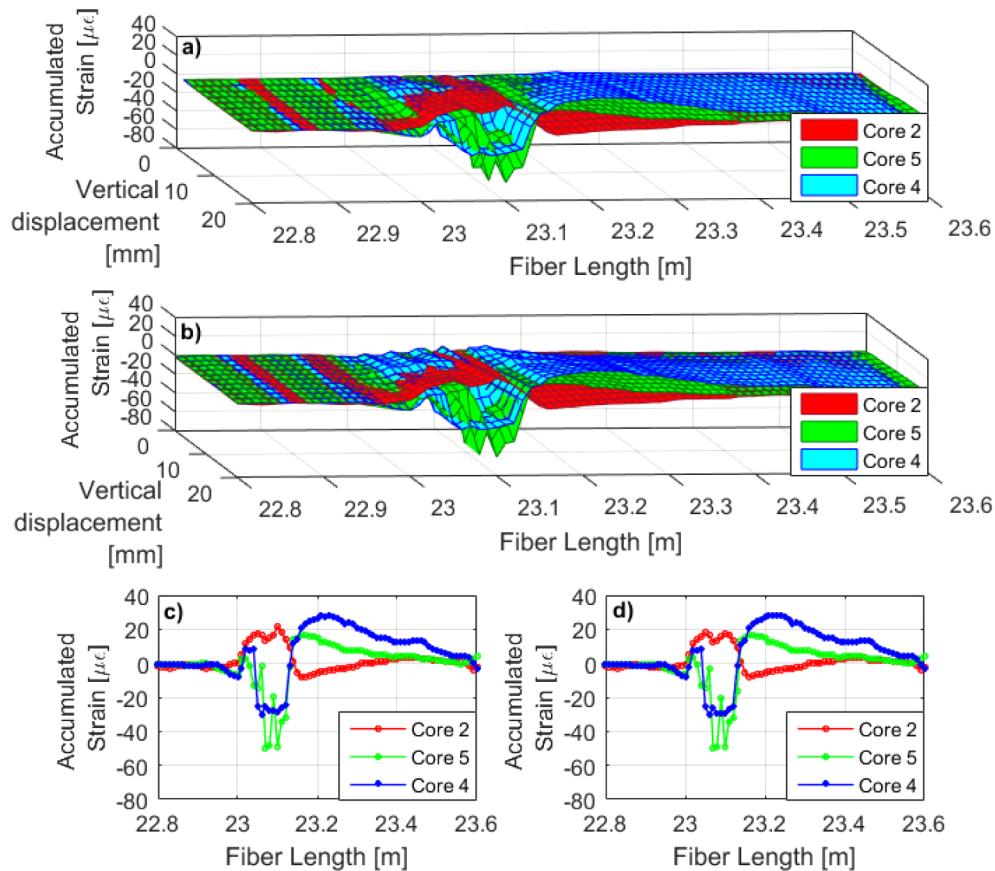
Fig. 5. (a) and (c) Accumulated strain due to vertical displacement, estimated as the summation of the computed strain for each pair of vertical positions for three cores of the fiber. (b) and (d) 2D view of the accumulated strain as a function of the fiber length for a vertical displacement of 18 mm. In the upward displacement [(a) and (b)] the first reference sweep is carried out at the lowest point (set at 0 mm of relative vertical displacement) and consecutive measurements are obtained with upward displacements. In the downward displacement [(c) and (d)] the first measurement is obtained at the highest position (+20 mm of relative vertical displacement), while measurements are obtained with downward displacements.

From the strain (ε_b) values obtained for each core, and making use of the equations presented in section 2, the curvature (k) and the bend orientation (θ_b) of the fiber can be calculated along its entire length. Figure 6(a) shows the retrieved curvature change for several positions of the translation stage, beginning from the lowest vertical displacement (defined as 0 mm of relative displacement), going upward to the highest position (+20 mm) and returning downward through the same steps to the starting point. As expected, the obtained curvatures show strong repeatability in the upward and downward directions, though an increment in the error can be observed as the measurements advance. Curvature can have negative values starting from the inflection point if one is not considering the angle at which such curvature is changing. Absolute curvature change combined with angle measurement gives complete information about the relative shape. This is because the results are based on cumulative measurements, and due to the intrinsically-static acquisition time (each frequency scanning requires 270 steps), an incremental error is expected toward the end of the set of measurements. This error was quantified from the difference of the

upward and downward pair of measurements at a fixed fiber length of 23.25 m, and the results are illustrated in Fig. 6(b) as function of the measurement iterations. As can be seen, the greatest error is obtained for the last iteration, which corresponds to a vertical displacement of 2 mm in downward direction.
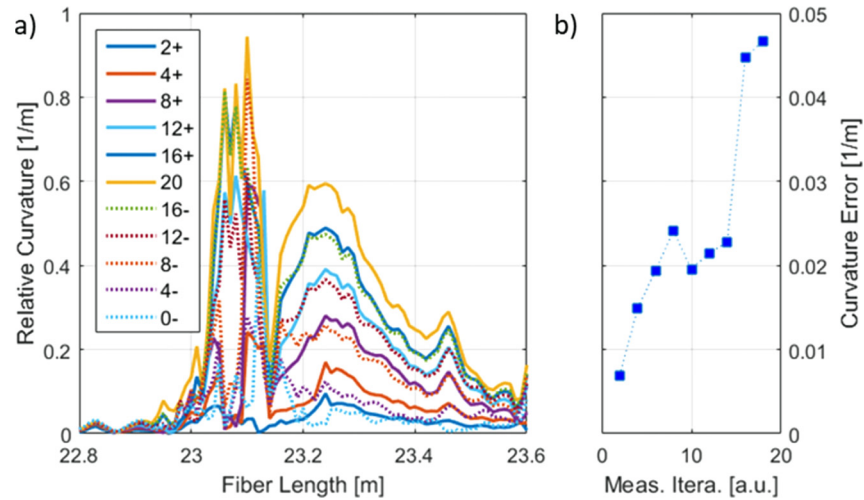

Fig. 6. (a) Measured relative curvature as a function of the fiber length for several positions of the moving stage, starting at the bottom (0 mm elevation), shifting upwards to 20 mm (continuous lines), and going back down to the original position (dotted lines). (b) Estimated curvature error as a function of the measurement iterations (the last iteration corresponds to the 2 mm vertical displacement in downward direction. This error was quantified from the difference of the upward and downward pair of measurements at a fixed fiber length of 23.25 m) .

On the other hand, Fig. 7 similarly depicts the calculated bend orientation as a function of the fiber length for the same steps of the translation stage. As can be seen, the orientation of the piece of fiber that is lying on the base, i.e., from 22.8 m to ~ 22.95 m (point A in Fig. 3), remains
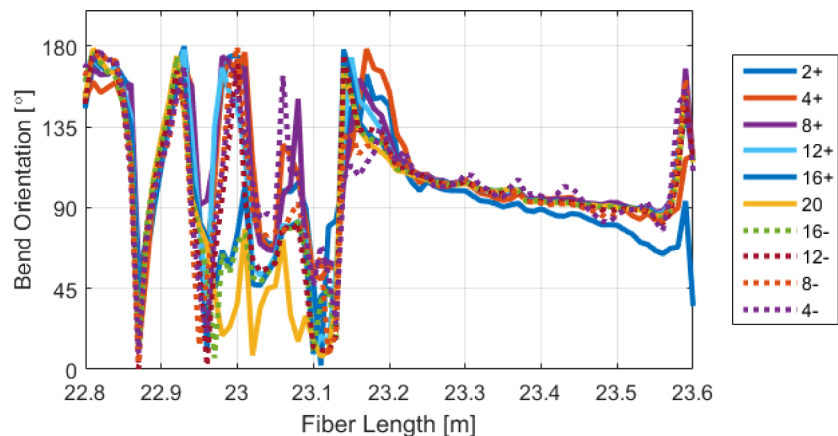

Fig. 7. Bend orientation as a function of the fiber length for several relative vertical positions of the moving stage, starting at 0 mm, shifting upwards to 20 mm (continuous lines), and going back down to the original position (dotted lines).

unchanged over the whole set of measurements. This result is expected as this fiber segment is fixed to the base, and it is not exposed to any change. Beyond ~ 22.95 m from the far end of the fiber, the computed bend orientation of the fiber appears to be random, showing a strong change in orientation before the curvature sign change (inflection point at ~ 23.16 m), and later a smoother shift until the fiber end. However, it can be seen that the pair of results obtained for the same vertical position show a similar profile, which proves the repeatability of the system. An exception can be observed in the last measurement referring to a relative vertical displacement of 4 mm in the downward direction (4 mm – in Fig. 7), which corresponds to the position with the highest cumulative error. This error is particularly clear after the curvature sign change, where several spurious peaks appeared. The biggest curvature changes seen from point 23.15 correspond to the well-defined constant angle measurement. The discontinuities seen before this point are in line with what would be expected in an angle change graph and whilst this looks like noise, in fact it is not, as illustrated by the repetitive nature of the measurements. Rapid changes in fiber bending orientation seen from ~ 22.95 m to ~ 23.1 m correspond to fast changes in curvature measurements form Fig. 6a). Such measurement can be explained by the influence of protective tape mechanical properties. Well defined curvature measurements correspond to well defined bend orientation. Such areas have the biggest impact on end shape change calculation.

Finally, the changes of the fiber shape are calculated by means of the Frenet-Serret formulas. The results obtained for each height-position are illustrated in Fig. 8 as a 3D graph and for two different perspectives. The offset axis represents a change in the fiber-end-position in an additional dimension caused by instabilities in the setup (for an ideal vertical translation of the
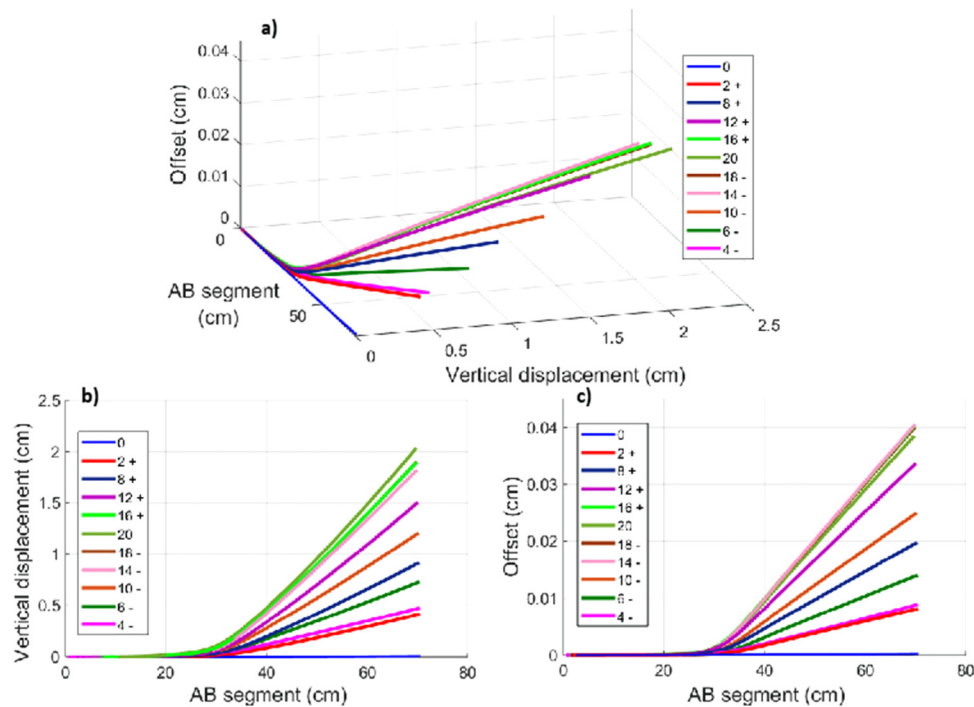

Fig. 8. (a) 3D illustration of the retrieved shape of the fiber for different vertical positions in steps of 2 mm (positive sign: upward displacement; negative sign: downward displacement). (b) and (c) shape of the fiber as a function of the vertical displacement and the offset respectively. The offset axis corresponds to a change in the fiber-end-position in an additional dimension caused by instabilities in the setup.

fiber, the change in this axis would be null). The original position of the fiber (0 mm) is depicted as a blue line over the AB-segment axis, and it is used as the reference for the following shapes of the fiber. As can be seen, the obtained fiber shapes resemble successfully the changes in form applied to the fiber by adjusting its vertical position, though a cumulative error is still present in the last measurement (4 mm in downward direction). These results demonstrate the great sensitivity of the proposed technique, verifying that changes as small as 0.05 mm in the position of the far end of the fiber can be tracked efficiently over a 60 cm-long fiber. These small errors in the retrieved positions are mainly due to the small instabilities caused by the movement of the translation stage in a non-vertical direction, and yet, they are detected by this highly-sensitive system.

It must be highlighted that it is straightforward to overcome strain-temperature cross-sensitivity issues affecting φ-OTDR measurements with the proposed technique. Indeed, while different strain values are expected to be measured in every core of the MCF when changing the shape of the fiber, any temperature change can be simultaneously measured by all fiber cores. By detecting the common variations of the cross-correlation spectral peaks of each core used in the measurements, temperature changes can be easily identified. Additionally, it must be taken into account that the central core of the MCF is in a neutral position, which is essentially affected by the net longitudinal strain variations (not by the differential strain exploited here for shape sensing) and temperature variations, which can be used to compensate the relative strain variations measured along the side cores.

5. Conclusion

A highly-sensitive distributed shape sensor based on φ-OTDR in a MCF has been proposed and validated, for the first time to the best of our knowledge. A high precision setup for differential strain distribution measurements has been implemented demonstrating a high strain sensitivity (down to ~0.3 $\mu\varepsilon$) over a 24 m-long MCF with a spatial resolution of 10 cm. Experimental calculations of the cumulated strain, curvature and bend orientation of the fiber have been carried out, confirming a good repeatability of the measurements. In addition, changes in the fiber shape have been successfully retrieved from the analysis of just three cores of the fiber. The great sensitivity of the proposed system has been demonstrated by detecting submillimeter changes in the position of the fiber end (0.05 mm changes in a 60 cm-long fiber). In addition, the proposed scheme avoids the commonly faced issues of cross-sensitivity between strain and temperature, due to its differential working principle. The results presented here illustrate the promising capabilities of the use of specialty optical fibers for distributed sensing, establishing the foundations of a broad range of interesting new applications, such as dynamic and 3D shape sensing. Since the proposed technique is based on conventional φ-OTDR measurements, the method can be straightforwardly applied for long-range distributed shape sensing over tens of kilometers.

Funding

References

1. X. Bao and L. Chen, "Recent Progress in Distributed Fiber Optic Sensors," Sensors **12**(7), 8601–8639 (2012).
2. A. H. Hartog, *An Introduction to Distributed Optical Fibre Sensors* (Taylor & Francis Group, 2017).
3. Z. Yang, M. A. Soto, D. M. Chow, P. Ray, and L. Thevenaz, "Brillouin Distributed Optical Fiber Sensor Based on a Closed-Loop Configuration," J. Lightwave Technol. **36**(5), 1239–1248 (2018).
4. A. Dominguez-Lopez, M. A. Soto, S. Martin-Lopez, L. Thevenaz, and M. Gonzalez-Herraez, "Resolving 1 million sensing points in an optimized differential time-domain Brillouin sensor," Opt. Lett. **42**(10), 1903 (2017).

5. I. Steinberg, L. Shiloh, H. Gabai, and A. Eyal, "Over 100 km long ultra-sensitive dynamic sensing via Gated-OFDR," *Proc. SPIE-24th Int. Conf. Opt. Fibre Sensors* 9634, 1–4 (2015).

6. A. Li, Y. Wang, Q. Hu, and W. Shieh, "Few-mode fiber based optical sensors," Opt. Express **23**(2), 1139–1150 (2015).

7. L. Zou, X. Bao, S. Afshar V, and L. Chen, "Dependence of the Brillouin frequency shift on strain and temperature in a photonic crystal fiber," Opt. Lett. **29**(13), 1485–1487 (2004).

8. J. Villatoro, V. Finazzi, V. P. Minkovich, V. Pruneri, G. Badenes, and J. Villatoro, "Temperature-insensitive photonic crystal fiber interferometer for absolute strain sensing," Appl. Phys. Lett. **91**(9), 091109 (2007).

9. Y. Lin, W. Jin, F. Yang, Y. Tan, and H. L. Ho, "Performance optimization of hollow-core fiber photothermal gas sensors," Opt. Lett. **42**(22), 4712–4715 (2017).

10. L. Zhang, Z. Yang, Ł Szostkiewicz, K. Markiewicz, T. Nasilowski, and L. Thévenaz, "Fully distributed pressure sensing with ultra-high-sensitivity using side-hole fibers," *Proc. 26th Int. Conf. Opt. Fiber Sensors*, 1–4 (2018).

11. B. De Pauw, S. Goossens, T. Geernaert, D. Habas, H. Thienpont, and F. Berghmans, "Fibre bragg gratings in embedded microstructured optical fibres allow distinguishing between symmetric and anti-symmetric lamb waves in carbon fibre reinforced composites," Sensors **17**(9), 1948 (2017).

12. Y. Lin, F. Liu, X. He, W. Jin, M. Zhang, F. Yang, H. L. Ho, Y. Tan, and L. Gu, "Distributed gas sensing with optical fibre photothermal interferometry," Opt. Express **25**(25), 31568–31585 (2017).

13. A. Ziolowicz, M. Szymanski, L. Szostkiewicz, T. Tenderenda, M. Napierala, M. Murawski, Z. Holdynski, L. Ostrowski, P. Mergo, K. Poturaj, M. Makara, M. Slowikowski, K. Pawlik, T. Stanczyk, K. Stepien, K. Wysokinski, M. Broczkowska, and T. Nasilowski, "Hole-assisted multicore optical fiber for next generation telecom transmission systems," Appl. Phys. Lett. **105**(8), 081106 (2014).

14. Y. Kokubun and M. Koshiba, "Novel multi-core fibers for mode division multiplexing: Proposal and design principle," IEICE Electron. Express **6**(8), 522–528 (2009).

15. G. M. H. Flockhart, W. N. MacPherson, J. S. Barton, J. D. C. Jones, L. Zhang, and I. Bennion, "Two-axis bend measurement with Bragg gratings in multicore optical fiber," Opt. Lett. **28**(6), 387–389 (2003).

16. L. Yuan, J. Yang, Z. Liu, and J. Sun, "In-fiber integrated Michelson interferometer," Opt. Lett. **31**(18), 2692–2694 (2006).

17. A. Fender, W. N. MacPherson, R. R. J. Maier, J. S. Barton, D. S. George, R. I. Howden, G. W. Smith, B. J. S. Jones, S. McCulloch, X. Chen, R. Suo, L. Zhang, and I. Bennion, "Two-axis accelerometer based on multicore fibre Bragg gratings," IEEE Sens. J. **8**(7), 1292–1298 (2008).

18. L. Yuan, J. Yang, and Z. Liu, "A compact fiber-optic flow velocity sensor based on a twin-core fiber Michelson interferometer," IEEE Sens. J. **8**(7), 1114–1117 (2008).

19. Z. Zhao, M. A. Soto, M. Tang, and L. Thévenaz, "Distributed shape sensing using Brillouin scattering in multi-core fibers," Opt. Express **24**(22), 25211–25222 (2016).

20. Y. Koyamada, M. Imahama, K. Kubota, and K. Hogari, "Fiber-optic distributed strain and temperature sensing with very high measurand resolution over long range using coherent OTDR," J. Lightwave Technol. **27**(9), 1142–1146 (2009).

21. M. P. Do Carmo, *Differential Geometry of Curves and Surfaces* (Prentice-Hall, Inc, 1976).

22. J. P. Moore and M. D. Rogge, "Shape sensing using multi-core fiber optic cable and parametric curve solutions," Opt. Express **20**(3), 2967–2973 (2012).

23. G. P. Agrawal, *Nonlinear Fiber Optics* (Elsevier Inc., 2007).

24. H. F. Martins, S. Martin-Lopez, P. Corredera, M. L. Filograno, O. Frazao, and M. Gonzalez-Herraez, "Coherent noise reduction in high visibility phase-sensitive optical time domain reflectometer for distributed sensing of ultrasonic waves," J. Lightwave Technol. **31**(23), 3631–3637 (2013).